Polymer/Nanographite Composites for Mechanical Impact Sensing

Maris Knite and Artis Linarts

Abstract The purpose of this chapter is to give a review of the polymer/nanographite composite (PNGC) materials specially developed for applications in mechanical strain and pressure sensors that can be used for design of flexible sensing systems. Our recent achievements in design, processing, and investigation of physical properties of elastomer and nanostructured carbon composites as prospective materials for mentioned sensors are also presented. In the beginning, theoretical principles of tunneling percolation theory and piezoresistivity have been described. We discuss the most suitable polymer matrices and electrically conductive nanographite fillers for sensitive PNGC. Preparation methods of mechanically sensitive PNGC have been considered. Different particularly produced and tested polymer/nanographite composites are overhauled and possible advantages and disadvantages of PNGC in different possible applications are analyzed.

Keywords Strain · Pressure · Sensors · Electronics

1 Introduction

The purpose of this chapter is to give a review of the polymer composite materials developed directly for application in strain and pressure sensors by using different nanographite structures as filler. We understand with the term "nanographite" the following fillers: extra-conductive highly structured carbon black (HSCB), carbon nanotubes (CNT), thermally exfoliated graphite (TEG) as well as the recently developed graphene. All of them have sp^2-hybridized crystal structure like graphite, and at least one dimension is smaller than 100 nm. Extra-conductive carbon black can be attributed to nanographite because its primary nanoparticle faces

M. Knite (✉) · A. Linarts
Institute of Technical Physics, Riga Technical University, 14/24 Azenes Street, Riga LV-1007, Latvia
e-mail: Maris.Knite@rtu.lv

K.K. Sadasivuni et al. (eds.), *Graphene-Based Polymer Nanocomposites in Electronics*, Springer Series on Polymer and Composite Materials,
DOI 10.1007/978-3-319-13875-6_9

consist of graphene platelets [1] or have "graphitic like organization" [2]. Our recent achievements in design, processing, and investigation of physical properties of elastomer and nanographite composites as prospective materials for mechanical (pressure, strain) indicators are also presented in this chapter.

Piezoelectric ceramics or constantan-chromium-alloy-based strain gauges are widely used as mechanical impact (MI) sensors. Such sensors are separate units from the monitored material or structure. There is a demand for new flexible large area sensors that could be easy embedded in different integrities and used for sensing multiple locations. High elasticity (hyperelasticity) polymer matrix based materials are still of interest. All of flexible polymer composite materials developed for MI sensing can be generally classified as electrically active (electronic response) or optically active (photonic response) materials. An example of a photonic response polymeric composite transducer for tactile sensing is based on optical fiber with Bragg grating embedded in polydimethilsiloxane [3]. The basic principle of this transducer lies in the monitoring of the wavelength shift of the returned Bragg-signal as a function of the strain or force. Comprehensive picture of current status of micro- and nanostructured flexible optical fiber sensors with particular reference to surface plasma resonance fiber sensors and photonic crystal fiber sensors is given by Fortes et al. [4], Yan et al. [5] and Lee et al. [6].

In the present chapter, we concentrate on smart polymer/nanographite composites (PNGC) that can give considerable electrical response to mechanical impact.

In the first section, the theoretical aspects of tunneling percolation as well as mechanical impact sensing mechanisms for PNGC based on quantum tunneling effect are going to be discussed. Thermodynamic force–response aspects of piezoresistivity are also presented.

In the second section, the most suitable nanographite filler materials, polymer matrix materials, and methods of preparation as well as principle of design of most sensitive PNGC are analyzed.

The third section informs about the most interesting PNGCs developed and investigated somewhere for mechanical impact sensing.

Our recent achievements in development of polymer/nanographite composite sensor-element systems for mechanical impact sensing as well as survey of particular technical solutions for sensing systems are given in the fourth section.

2 Theoretical Aspects of Mechanical Impact Sensing by Polymer/Nanographite Composites

2.1 Principles of Tunneling PercolationTheory

Conductive polymer composite for strain sensing can be obtained when particles of good conductors (carbon black, graphite powder, particles of metals, carbon nanotubes, graphene i.e.) are randomly inserted into an insulating polymer matrix. A continuous insulator–conductor transition is observed in two-component

systems at gradual increase of the number of randomly dispersed conductor particles in an insulator matrix. Most often such transitions called percolation transitions are described by the model of statistical percolation [7, 8]. The volume concentration of conductor particles ϕ_C at which the transition proceeds is called percolation threshold or critical point. According to the statistical model, conductor particles, in the vicinity of ϕ_C, assemble in clusters and the correlation radius ζ (average distance between two opposite particles of a cluster) diverges as

$$\xi \sim |\phi - \phi_c|^{-\nu} \quad \text{if } \phi > \phi_c \tag{1}$$

upon approaching ϕ_C (ν—critical indices) [7].

In the vicinity of percolation threshold, electric conductivity σ of the composite changes as:

$$\sigma \sim |\phi - \phi_c|^{t} \quad \text{if } \phi > \phi_c \tag{2}$$

here t—critical index [8]. Balberg et al. [9] developed a theory for percolation-like behavior for polymer and conductive nanoparticle composites where interparticle charge tunneling considerably prevailed against direct (geometrical) interparticle contacts. It was found that Eq. (2) can still be used for such tunneling supported percolation system only the nonuniversal behavior of critical index t should be taken into account [9]. It means that the experimentally obtained values of t remarkably differ from the "universal" value $t = 2$. When such conductive composites are mechanically stressed, then the both ξ and σ change correspondingly. This is the reason of piezoresistance (the resistance changes vs. mechanical strain) effects. Changes of electric resistance with strain and pressure can be simply explained on microscopic level as a result of the percolation structure change of conductive particles network (destruction or formation of conductive micro- and nanochannels).

New interesting properties are expected in case when the composite contains dispersed nanosize extra-conducting particles [10]. Polymer/electroconductive nanostructure composites offer attractive alternatives for developing new generation of flexible large-size sensors because of their superior mechanical and electrical properties.

2.2 Charge Tunneling Models of Piezoresistivity

The phenomenon where the electrical resistivity of a material changes due to applied mechanical stress is called piezoresistivity. Correct theoretical description of piezoresistivity on macroscopic or phenomenological level has been done by Rocha et al. [11]. They developed piezoresistive coefficient tensor that describes all possible mechanical force effects on the electric resistivity of a composite with only one term "piezoresistivity". In the scientific literature term, "tensoresitivity" has also been used by some authors [10, 12]. If the resistivity changes under tensile force such material exhibits the tensoresistivity effect. For better

understanding the particular manifestation of piezoresistivity in PNGCs, in this chapter, we propose to use terms “pressure coefficient of resistance” or “tension coefficient of resistance” like “temperature coefficient of resistance” used for characterization of temperature dependence of resistance on materials. So, it is possible to distinguish four different experimentally observed cases of resistivity change under MI forces:

1. negative pressure coefficient of resistance (NPR) when the resistivity decreases with compressive force [13, 14];
2. positive pressure coefficient of resistance (PPR) when the resistivity increases with compressive force [10, 14, 15];
3. positive tension coefficient of resistance (PTR)—resistivity rises by tensile strain [10]
4. negative tension coefficient of resistance (NTR) if the resistivity under stretching force decreases [16].

Generally speaking all of the above-mentioned effects of mechanical impact on mechanoelectrically active polymer composites can be explained by changes of nanodimensional structure of electroconductive nanoparticle grid inside the polymer matrix. If the inter-particle distance rises or the number of conductive channels diminishes, the resistivity of the sample rises (PPR and PTR). If the interparticle distance decreases or the number of conductive channels increases, the resistivity of sample decreases (NPR and NTR). Further, in this section, we report the more exhaustive theoretical explanations of all four effects on microscopic level based on quantum charge tunneling.

Theoretical description of NPR effect experimentally observed in polymer/metallic microparticle composites has been done by Zhang et al. [13] based on early developed theory for tunneling conductivity between dissimilar electrodes separated by a thin insulating film [17].

Knite et al. [10] modified the previously mentioned charge tunneling theory for experimentally observed reversible PTR effect in polyisoprene/HSCB composites. To explain the large PTR and PPR effects Knite et al. [10] assumed that bonds between the nanostructured agglomerates of carbon black and the hyperelastic polymer chains are stronger compared to the bonds between carbon nanoparticles themselves. Possibly, they are bonded by the free radicals of the chains thermally activated at vulcanization. At stretching of the composite, the carbon agglomerates remain covalently bonded to the polymer chains, as they are dragged along with the polymer chains and pulled apart. In case of poorly structured or microsize carbon filler, the bonding between carbon particles and polymer chains is weak and the filler makes irreversible (rigid and rather immobile) clusters in the insulating matrix. The effects are irreversible. In case of (HSCB) like PRINTEX-XE2, after the stretch is released, the contacts between carbon agglomerates are restored as the polymer chains return practically to its original positions [10].

The total electrical resistance of conductor-filled polymer composite is a function of both the resistance of each conducting particle and of the polymer matrix. As the conductivity of the conducting particles is very large in comparison to that

of the polymer matrix, the resistance across the particles may be neglected. When particles are separated far enough from each other, no current flows through the composite. If the distances separating particles are small, tunneling currents may arise.

According to the model derived by Zhang et al.[13], the total electrical resistance R of the composite is calculated as:

$$R = \left(\frac{n}{N}\right)\left(\frac{8\pi hs}{3a^2\gamma e^2}\right)\exp(\gamma s), \tag{3}$$

where n is the number of particles forming a single conducting path, N—the number of conducting paths, h—Plank's constant, s—the least distance between conductive particles, a^2—the effective cross-section, where tunneling occurs, e—the electron charge, and γ is calculated as:

$$\gamma = \frac{4\pi(2m\phi)^{0.5}}{h}, \tag{4}$$

where m is the electron mass and ϕ—the height of potential barrier between adjacent particles.

If stress is applied to a composite sample, the resistance will be altered due to the change of particle separation. Assuming that under applied stress, the particle separation changes from s_0 to s, the relative resistance (R/R_0) is given by

$$\frac{R}{R_0} = \left(\frac{s}{s_0}\right)\exp\left[\gamma(s - s_0)\right] \tag{5}$$

where R_0 is the initial resistance, and s_0—the initial particle separation [13]. In case of elastomer composite, the separations under tensile strain is calculated as

$$s = s_0(1 + \varepsilon) = s_0\left[1 + \left(\frac{\Delta l}{l_0}\right)\right] \tag{6}$$

where ε is the tensile strain of the elastomer matrix, Δl—deformation of the composite sample, and l_0—initial length of the sample. Substitution of Eq. (6) into Eq. (5) yields

$$\ln R = \ln R_0 + \ln\left[1 + \left(\frac{\Delta l}{l_0}\right)\right] + A_0\left(\frac{\Delta l}{l_0}\right) \tag{7}$$

where $A_0 = \gamma s_0$.

It was shown [10] that the model of tunneling currents quite well describes the experimental data at small deformations $\Delta l/l_0 < 0.1$ with $A_0 = 6.491$ and $R_0 = 3.770 \times 10^5\ \Omega$. Knite et al. [10] proposed that the high rate of the increase of R/R_0 at larger deformations $\Delta l/l_0$ is related to destruction of the conducting network, i.e., with decrease of the number of conducting paths N:

$$N = \frac{N_0}{\exp\left[A_1\left(\frac{\Delta l}{l_0}\right) + B\left(\frac{\Delta l}{l_0}\right)^2 + C\left(\frac{\Delta l}{l_0}\right)^3 + D\left(\frac{\Delta l}{l_0}\right)^4\right]} \tag{8}$$

where N_0 is the initial number of conducting path, A_1, B, C, and D all are constants [10].

The substitution of Eq. (8) into Eqs. (3) and (7) yields

$$\ln\left(\frac{R}{R_0}\right) = \ln\left[1 + \left(\frac{\Delta l}{l_0}\right)\right] + A\left(\frac{\Delta l}{l_0}\right) + B\left(\frac{\Delta l}{l_0}\right)^2 + C\left(\frac{\Delta l}{l_0}\right)^3 + D\left(\frac{\Delta l}{l_0}\right)^4 \tag{9}$$

Equation (9) comprises both mechanisms—change of tunneling currents and disruption of tunneling currents in the conductive nanochannels. A good agreement between the theoretical and experimental curves have been achieved at $A = 8.206$; $B = -90.979$; $C = 873.911$; $D = -1{,}333.339$, and $R_0 = 3.835 \times 105\ \Omega$ for polyisoprene/HSCB composite [10].

At the first sight surprising surprising PPR effect in PNGC observed first by Knite et al. [10] has been later quantitatively explained by Zavickis et al. [18] by taking into account the transversal slippage that causes strain in the direction perpendicular to the applied axial pressure, which in turn provokes the tunneling barrier thickness increase at small deformations and subsequential rupture of the conductive channels in the direction perpendicular to the applied pressure at relatively larger strain. The exceptionally high structure of the conductive carbon black filler provides extremely entangled conductive grid structure and prevents new conductive pathways to develop in the direction parallel to the strain applied. Based on this, Zavickis et al. [18] adopted a more advanced theoretical model that describes the dependence of electrical resistivity directly on operational pressure for piezoresistive PNGC. This was done to simplify future calculations, since to characterize piezoresistive properties of PNGC the pressure is the primary argument instead of deformation. In case of compression of the elastomer matrix, authors considered the transversal elongation of the sample, thus the separations between adjacent particles can be calculated as

$$s = s_0\left(1 + \varepsilon^{\perp}\right) = s_0\left[1 + \left(\frac{\Delta L'}{L_0'}\right)\right], \tag{10}$$

where $\varepsilon^{\perp}$ is the transversal strain of the matrix in the perpendicular direction to applied axial pressure force, $\Delta L'$—transversal deformation of the sample, and L_0'—transversal length of the sample. Zavickis et al. [18] proposed that the relative elongation of the sample in the direction perpendicular to applied axial pressure $\Delta L'/L'_0$ can be expressed as follows:

$$\frac{\Delta L'}{L_0'} = -\left(-\nu\frac{\Delta L}{L_0}\right) = \nu\frac{P}{\lambda}, \tag{11}$$

where ν—Poisson ratio, λ—elastic modulus of composite, P—compressive pressure on the sample, and $-\Delta L/L_0$ is the negative elongation (reduction) in the

direction parallel to applied compressive force. After taking into account Eqs. (10) and (11), Zavickis et al. [18] got equations similar to Eqs. (7) and (9), respectively:

$$\ln R = \ln R_0 + A_0' P \tag{12}$$

for small values of pressure (small deformations) and

$$\ln R = \ln R_0 + A' P + B' P^2 + C' P^3 + D' P^4 \tag{13}$$

for large values of pressure (large deformations), where

$$A_0' = A_0 \frac{\nu}{\lambda}, \quad A' = A \frac{\nu}{\lambda}, \quad B' = B\left(\frac{\nu}{\lambda}\right)^2, \quad C' = C\left(\frac{\nu}{\lambda}\right)^3 \quad \text{and} \quad D' = D\left(\frac{\nu}{\lambda}\right)^4.$$

To verify the assumptions in the theoretical description of the PPR effect, Zavickis et al. [18] fitted the experimental data points of the first upgoing cycle using Eqs. (12) and (13) and near perfect agreement was found between the two theoretical curves and the corresponding experimental values (Fig. 1). This was done for the operational pressure range of up to 4.1 bar where, according to approximate calculations, relative unidimensional axial compressive deformation of the sample is considered to be less than 10 %, which should correspond to the elastic deformation region.

Developed by Knite et al. [10], the combined piezoresistance model based on both the tunneling effect and the destruction of conducting paths have been modified and used also by other authors for theoretical description of different piezoresistance effects in some PNGCs [15, 19–21]. In two cases, our combined piezoresistance model was successfully applied for elastomer/graphite nanosheet composites [15, 20].

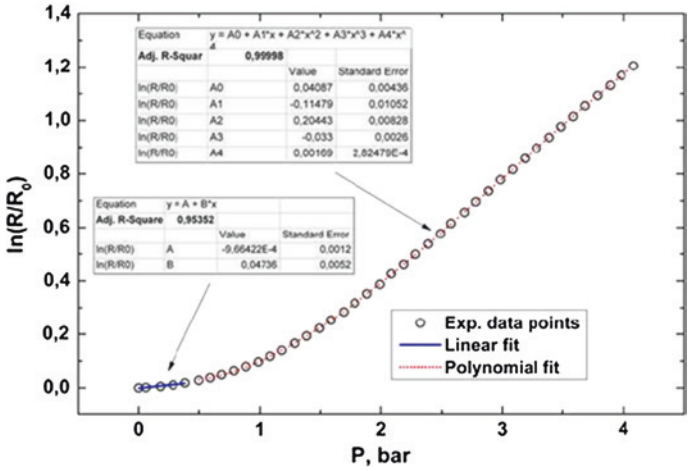

Fig. 1 A linear (12) and a fourth-order polynomial (13) fit to the experimentally observed positive piezoresistivity of a completely flexible sensor prototype [18]. Copyright 2011. Reproduced with permission from Elsevier Ltd

Wang Luheng et al. [19] generalized Eq. (9) for both PPR and NPR effects observed experimentally in the same kind of silicone rubber/HSCB composites but with different concentration of HSCB. The PPR effect has been observed in PNGCs with low mass ratio of HSCB to silicone rubber F ($0.08 \leq F \leq 0.09$) but NPR—in PNGCs with ($0.14 \leq F \leq 0.24$). These experimental results were explained by analyzing the changes due to the applied pressure in the gap sizes in the existing effective conductive paths and in the number of effective conductive HSCB paths in the composite samples [19].

Surprising at first, a NTR effect has been observed and qualitatively (non-numerically) explained by Flandin et al. [16] in case of ethylene-octene elastomer (EO)/HSCB composite. Authors (Flandin 2001 Polym) reported that the EO filled with HSCB exhibits a reversible decrease in resistivity under stretching with up to 30 % strain. In addition, these characteristics have been observed only in high-structure carbon black, as composites of the EO elastomer with low-structure carbon black or carbon fibers exhibited conventional PTR behavior [16]. An explanation was given by taking into account the unique features of both filler and matrix as follows. In contrast to covalently cured (chemically cross-linked) elastomers, the structural basis for EO elastomers is provided by a network of flexible chains with fringed micellar crystals (physically cross-linked). Authors believe that upon stretching, the fringed micellar junctions of EO elastomers do not remain fixed, but slide by a process of detachment–attachment, which can also be considered as partial melting. Due to local stress concentrations, the actual strain in the vicinity of the carbon particle can be noticeably higher than the average macroscopic strain. Therefore, the crystalline junctions can "melt" and flow out from the space between nearby particles. Either an existing pathway is improved by a rise in the charge tunneling conductivity or a new electrical pathway is thus created. Particularly interesting for strain gauge applications was a reversible and strain-rate independent decrease in resistivity with up to 30 % strain [16].

2.3 The Shift of Percolation Threshold Under External Thermodynamic Forces

From the macroscopic point of view, the principle of strain sensing is based on the shift of the percolation threshold due to some thermodynamic forces, for example, under tensile strain as shown in Fig. 2.

One can see that due to the shift of percolation threshold under 40 % strain the electric resistance changes more than 10^4 times for composite with 10 phr (parts per hundred rubber) of nanostructured carbon black. The maximum strain sensitivity is identified in the percolation region (9–11 mass parts of filler) for relaxed PNGC (Fig. 2). Thus, one may expect the maximum sensitivity of PNGC materials to the external thermodynamic forces in filler concentration region slightly above the percolation threshold of electric conductivity as demonstrated by Knite et al. [10].

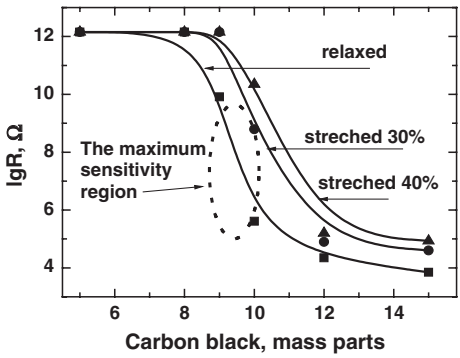

Fig. 2 Shift of the percolation threshold under tensile strain in the polyisoprene/high-structure carbon nanoparticles composite [22]. Copyright 2007. Reproduced with permission from Elsevier Ltd

3 Principles of Design and Characterization of Polymer/Nanographite Composites for Mechanical Impact Sensing

3.1 Most Suitable Filler Materials

In this chapter, we describe only such sp^2 hybrid carbon nanostructures (nanographites) that can be attributed to 2D nanostructures and we are going to pass the 1D ones like carbon nanotubes (CNT). One can find useful information about polymer/CNT composites developed for mechanical impact sensing in review papers [23, 24].

3.1.1 Extra-Conductive Carbon Black as Nanographite Filler

HSCB PRINTEX XE2 (ECB) is a commercially provided nanographite filler that is used in most cases for elaboration the PNGC [10, 25]. Several authors [1, 2] have reported a graphite-like organization of carbon atoms in HSCB nanoparticles near surface. In Fig. 3 one can see the polyhedron-like shape of primary particles of HSCB that is an indirect verification of the nanographite structure of HSCB. We believe that the faces of primary carbon nanoparticle consist of graphene nanoplatelets. Another indirect evidence for this is the high value of electric conductivity in comparison with other technical carbon blacks.

3.1.2 Thermochemically Exfoliated Graphite

Graphene is a single layer of sp^2-bonded carbon atoms that can be thought of as an individual atomic plane extracted from graphite [27]. Recent studies [28–30] have demonstrated that several stacked graphene layers, which essentially represent partially exfoliated graphite, can be applied successfully as fillers for polymeric

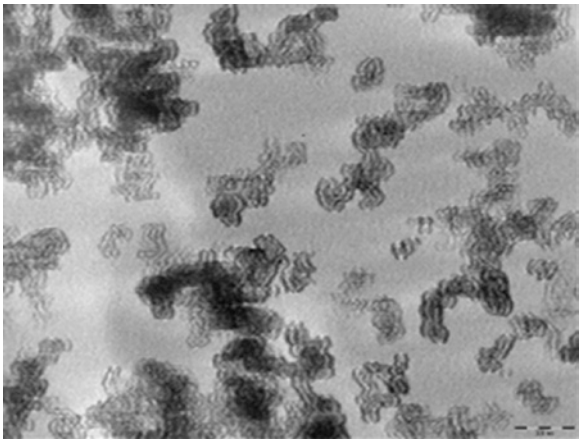

Fig. 3 TEM image of high-structured carbon black nanoparticle PrintexXE2 . Scale mark 200 nm [26]. Copyright 2007. Reproduced with permission from Elsevier Ltd

matrices. Thermochemically exfoliated graphite (TEG) produced from graphite subjected to thermal shock is shown lower on Fig. 10.

3.2 Most Suitable Matrix Materials

The polymer elastomers are the most useful matrix materials for the development of sensing elements intended for recurrent detection of large-scale mechanical impact there for they require reversible piezoresistive effect. For this purpose, the natural polyisoprene rubber has been found as the most promising matrix [10]. Silicone rubber also has been used as hyperelastic matrix for PNGC development [15, 19].

General principles of designing the structure of materials with the highest sensitivity that we adapted in this chapter for obtaining most sensitive multifunctional elastomer/nanographite composites are as follows:

1. Polyisoprene (natural rubber) with the best hyperelastic properties has to be chosen as the matrix material;
2. High-structured graphitized carbon nanoparticles (HSNP) (for example Printex XE2) providing a fine branching structure and a large surface area (better adhesion to polymer chains compared to low-structure graphitized nanoparticles (LSNP); short CNTs or small-size graphene platelets should be taken as filler. Because of a higher mobility of HSNP compared with LSNP, the electroconductive network in the elastomer matrix in this case is easily destroyed by very small tensile or compressive strain. We suppose this feature makes the elastomer–HSNP composite an option for more sensitive tactile elements.
3. The highest sensitivity is expected in the filler concentration region slightly above percolation threshold of a relaxed polyisoprene composite. The smallest mechanical strain or swelling of the composite matrix remarkably and

reversibly increases the resistance of such a composite. The sharper is the percolation transition of insulator/conductive particle composite, the higher should be the compressive stress sensitivity of sensing element [10].

3.3 Preparation Methods of Composites

Piezoresistive composites composed by an insulating matrix and conductive filler have been widely studied in the past years. Various fillers, polymers, and production methods have been used to produce continuous electrically conductive networks throughout the insulating polymer matrix. Electrical conductivity parameters of these heterogeneous composites have been found to be strongly dependant on filler concentration, filler geometry, and even composite preparation methods.

Depending on whether or not specific solvents have been used to lower the viscosity of the polymer matrix, all composite production methods can be divided into two groups:

1. Use of conventional polymer/rubber processing equipment that does not uses solvents—the filler is mechanically mixed into polymer, includes usage of various mixing mills, kneaders, banbury mixers, and even extruders. The polymer viscosity is generally high (Fig. 4);
2. Usage of certain solvents to dissolve the matrix and the filler is added to the mixture afterward. Polymer viscosity is much lower (Fig. 5).

In general, conventional polymer/filler mixing equipment offers high processing amounts and rates however the homogeneity of the composite structure is far worse compared to the polymer dissolution methods. Figure 5 shows typical scheme of piezoresistive composite production. At first, polymer is dissolved in adequate solvent then filler is added to the mixture and stirred for a certain period, afterward the solvent has to be evaporated. Long durations and usage of sometimes harmful solvents are the only drawbacks for this method. Ultrasound homogenizer can be used to produce suspensions/colloids of fillers and solvents before mixing with dissolved polymer. However even after the ultrasound treatment particles tend to aggregate due to the high specific surface of the nanosize fillers intermolecular Van Der Waals forces. Functionalization of particle surface might overcome this problem; however, the surface modification degrades the electrical properties of fillers.

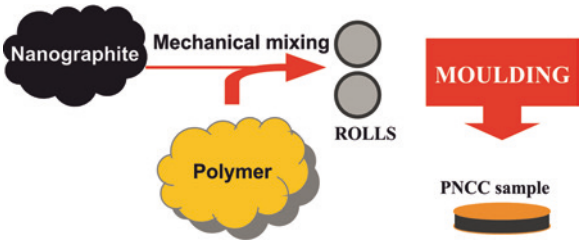

Fig. 4 Composite production scheme using conventional rubber processing equipment [25]. Copyright 2011. Reproduced with permission from lietuvos mokslų akademija

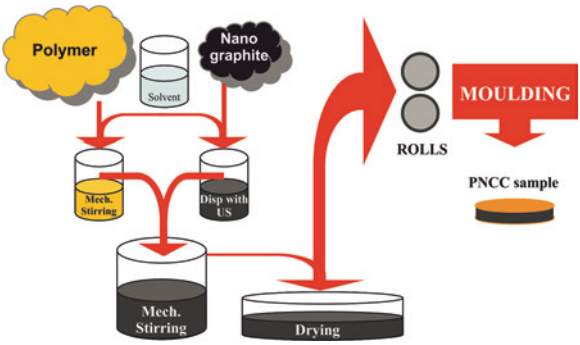

Fig. 5 Composite production scheme when the matrix is dissolved and then mixed with conductive filler [25]. Copyright 2011. Reproduced with permission from lietuvos mokslų akademija

4 Produced and Tested Polymer/Nanographite Composites for Mechanical Impact Sensing

4.1 Polymer/Extra Conductive (Graphitized) Carbon Nanoparticle Composites

Significant and reversible both PTR and PPR effects first were observed in polyisoprene/HSNP composites have been reported by Knite et al. [10]. Plates of 12 mm diameter were cut for piezoresistivty effect measurements from 1 mm thick 20 cm × 20 cm sheets vulcanized at high pressure. For studying the tensoresistivity effect 15 cm × 1.5 cm samples were cut. Copper foil electrodes were glued on both sides at sample ends and each pair of electrodes was shortcut by copper wiring. On a relaxed sample the distance between electrodes did not exceed 50 mm. Sandpaper was glued on the electrodes to fasten the samples in the stretching machine. Authors reported that of all the composites examined, the best results were obtained on samples with 10 phr of carbon nano-particles, which apparently belonged to the region of percolation phase transition. Electrical resistance of the samples increases by more than 4 orders upon a 40 % stretch (PTR effect) and more than 3 orders upon a 0.30 Mpa pressure (PPR effect) as seen in Fig. 6. Resistance practically returns to its previous value after the samples are relaxed (reversibility). The reversibility and the significant changes of electric resistance under both tensile and compressive strain were explained due to comparatively higher mobility of high structure nanoparticles compared to low structure particles as well as stronger adhesion of carbon nanoparticles to the polymer matrix compared to cohesion between nanoparticles themselves [10]. The growth of electric resistance with uniaxial stretching as well as with pressure can be explained as a result of destruction of the structure of the carbon electro-conductive nano size channel network. At low stretching deformation the experimental data has good coincidence with model of tunneling conductance [10], see also Eq. 7 in Sect. 2.2. The AC conductivity measurements also verify the tunneling model of conductance [10]. For description of the experimental results at high deformation

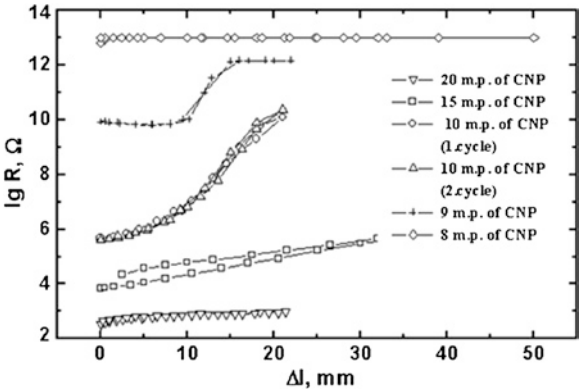

Fig. 6 Electrical resistance R of the nanocomposite as function of stretching deformation Δl at different phr (m.p.) of HSCB. On a relaxed sample the distance between electrodes was $l0 = 50$ mm, $T = 293$ K [10]. Copyright 2004. Reproduced with permission from Elsevier Ltd

the destruction of conductive network and decrease of conducting path have to be taken into account [10], see also Eq. 9 in Sect. 2.2. In case of uniaxial pressure (Fig. 7) destruction of electrically conductive channels is caused by deformation of the polyisoprene nanocomposite perpendicular to the direction of pressure (Eqs. 12 and 13, Sect. 2.2).

A tapping mode AFM Nanoscope III (Dimensions 3,000, Digital Instruments) was used to investigate the local nano-size properties of the polymers. The local conductivity patterns on the surface were studied on a modified conductive AFM. The AFM had standard silicon nitride cantilever tips. The AFM tip and cantilever were coated with a 5 nm thick Cr adhesive layer and a 15 nm thick Au layer. With a contact mode conductive atomic force microscope authors succeeded in obtaining a topographic picture of the sample surface and a nanoscale map of cross-sections of the electro-conductive channels and the insulating matrix of the same local spot. For example, it is seen in Fig. 8 that the extra-conductive carbon black nano-particles agglomerate during vulcanization process in clusters of size around 100 nm forming conductive channels throughout the whole sample. The blue regions in Fig. 8 represents insulating polyisoprene matrix and the red

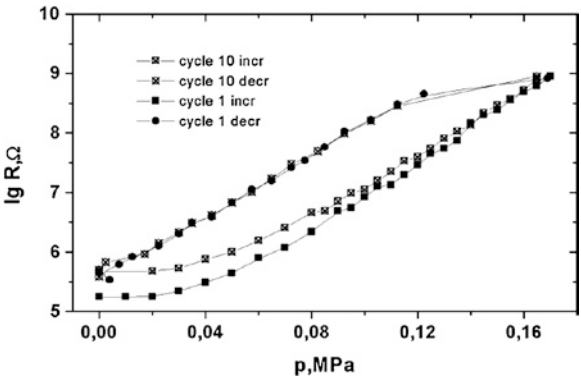

Fig. 7 Electrical resistance R of the 5-sheet nanocomposite block as function of uniaxial pressure p. The deformation of nanocomposite is constrained in the direction perpendicular to the acting force. $T = 291$ *K*. 293 K [10]. Copyright 2004. Reproduced with permission from Elsevier Ltd

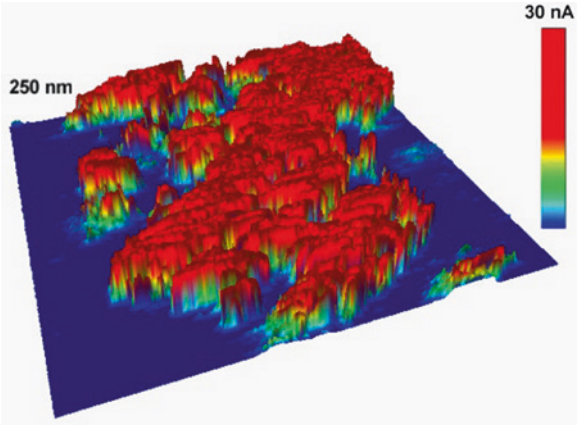

Fig. 8 Map of conductive channel sections of Polyisoprene matrix with 10 mass parts of nano-size carbon black. Relaxed state, $T = 294$ K, image size 250 nm [10]. Copyright 2004. Reproduced with permission from Elsevier Ltd

regions the electrically conductive HSNP channel sections on the surface of the PNGC sample [10].

The effect of a plasticizer on the change of the electrical resistance under deformation at strain was studied in polyisoprene composites containing dispersed HSCB at concentrations slightly above the percolation threshold [31, 32]. The addition of plasticizer to the initial materials increases the strain sensitivity of the composite and broadens the HSCB concentration interval of the percolation threshold. The observed improvements of the tensoresistive response are explained by decrease of cohesion forces between carbon nanoparticles and a higher mobility of the carbon nano-particles in the elastomer matrix in the presence of the plasticizer [31, 32].

Based on the PPR effect data Zavickis et al. [18] developed a completely soft matter hyper-elastic pressure (SHP) sensor prototype without any solid state (metallic) details. Sensor element is made using functional gradient multilayer approach, when elementary layers of PNGC with different conductive filler concentration are vulcanized together and forms uniform sensor body with integrated soft (hyper-elastic) electrodes as seen in Fig. 9.

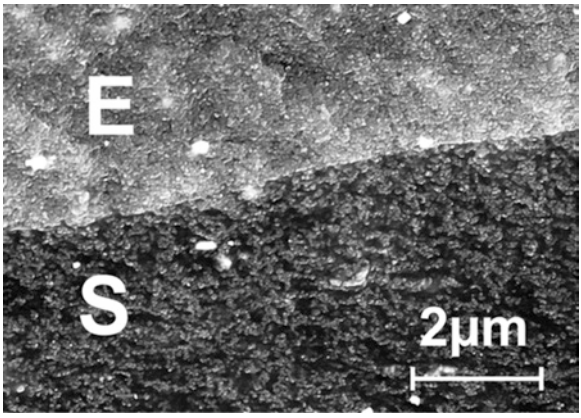

Fig. 9 The SEM picture of the interface between completely vulcanized sensor (*S*) and electrode (*E*) PNGC layers. Picture made from surface of the sample broken in liquid nitrogen [18]. Copyright 2011. Reproduced with permission from Elsevier Ltd

The SHP sensor element was made from 3 functional layers of PNGC, each with different concentration of HSCB: The pressure sensitive middle layer was chosen with 10 phr of HSCB that is slightly above previously obtained percolation threshold [10], to achieve maximal piezoresistivity of the structure. The electrode layers on both sides of the sensitive layer were chosen with comparably larger HSCB concentration, to promote good electrical conductivity. All the conductive parts were incorporated into dielectric natural rubber shell without any HSCB filler. Thin brass wires were used only for easy connection of the measuring equipment, but according to SHP concept, the electric wiring although can be made from conductive rubber strips, incorporated into dielectric shell. Corresponding components were pre-shaped using incomplete vulcanization in reduced vulcanization temperature and shorter curing times in hot steel mould, using high temperature resistive polymer film inserts to prevent sticking to mould during sample removal. Afterwards the pre-vulcanized components were assembled according to sequence mentioned above and cured until complete vulcanization [18]. The measured PPR effect in this prototype is shown on Fig. 1 and is theoretically explained by quantum tunneling effect (Eqs. 12 and 13, Sect. 2.2).

Zheng et al. [21] recently investigated the piezoresistive behavior of PNGC cast films and pressed films made from high-density polyethylene and PRINTEX XE-B. The mechanical and piezoresistive response were measured under axial tensile test and the PTR effect was observed for all samples tested. Authors stated that the normalized electrical resistance of the cast film was almost constant with strain in the elastic region of stress-strain curve and starts to increase with strain in the plastic region. Authors described these experimental results by successfully modifying the Eq. (9) (combined piezoresistance model based of both tunneling effect and destruction of conducting paths). It was also concluded that cast PNGC films could be potentially used as a strain sensor to identify the elastic and plastic deformation regions of the films [21].

4.2 Polymer/Graphite Nanosheet Composites and Polymer/Graphene Composites

In the latest review papers particulary devoted to tactile sensors [14, 33] as well as to development and application of graphene based polymer composites [34–36] only few research papers were analyzed regarding to use polymer/graphene composites in field of mechanical impact sensing. In this section we are going to attempt to fulfill this space. The use of graphene for the development of a strain and damage sensor to be utilized in structural health monitoring of fiber reinforced polymers was evaluated and modeled by Chiacchiarelli et al. [29]. An Epikote 862 diglycidyl ether of bisphenolF(DGEBF)epoxy resin, kindly supplied by Hexion, was used as a matrix. Diethyltol-uenediamin e (DETDA), supplied by Lonza, was used as curing agent (26.4 phr). Graphenenanoplatelets (GNPs) were supplied by Cheap Tube Inc. (Grade 2). According to the manufacturer, the

GNPs had a surface area of 100 m^2/g, an average thickness of around 10 nm and an average diameter of 25 μm. They were used as supplied by the manufacturer. Autors obtained colloidal suspension of GNPs in chloroform after sonication with a Vibracell® VC750 tip sonicator for 1 h at an amplitude of 30 % (225 W). Then, the epoxy monomer was added and the mixture was further sonicated for 1 h at identical conditions. Afterwards, in order to fully remove the solvent, the solution was heated on a hot plate (Infrared spectroscopy was used to corroborate solvent evaporation). Finally, the hardener was added and the system was magnetically stirred for 5 min. This reactive mixture was then used to create a coating (50 × 6 mm 2 area) onto the carbon fiber/epoxy composite (CFRC) specimens with previously prepared Al electrodes. Finally, the coated specimens were cured at130 °C for 5 h. The PTR effect of sensitive composite layer was measured CFRC bending test cycles. Authors observed reversible and irreversible behavior of sensor tensoresistivity. Authors explained both these behaviors by modifying Eqs. (7) and (8) respectively (Sect. 2.2). It was experimentally shown that both the stress and damage of the composite can be detected by a simple measurement of the sample electrical resistance change.

Lu et al. found that in high-density polyethylene graphite nanosheet (5–20 μm; 30–80 nm) composites there is a critical pressure at which the piezoresistive behavior changes from PPR effect to NPR effect. The HDPE and GNs were first wet-mixed to achieve a uniform dispersion and afterward mixed on a two-roll mill. The critical pressure value increases with increasing filler concentration and generally up to 10 Mpa pressure, the effect is negative due to a decrease of interparticle separation but at even higher pressures (up to 40 Mpa) the PPR effect has been stated reason for this is the large deformation of polymer matrix that leads to destruction of conductive channels [37]. However, the NPR effect at low pressures might be attributed to increased/better electrical contact area when pressure is applied since sensors' resistivity is measured between steel electrodes.

Chen et al. produced finger pressure-sensitive composite based on silicone rubber graphite nanosheets (5–20 μm; 30–80 nm) [15]. Percolation threshold for such composition was determined to be 0,9 vol%, a composite containing 1,36 vol% conductive filler was found to be the most sensitive to external pressure reaching R/R_0 values around 800,000 under 0.7 MPa pressure. Authors described the piezoresistive behavior by the tunneling models as well as used the models for change of the number conducting paths that are similar to model developed for polyisoprene high-structure carbon black composites [10]. In the same way as Knite et al. [10] stated for nanostructured carbon black, the authors [15] made conclusions that stronger adhesion of the GNs to the polymer matrix compared to the cohesion between the nanosheets themselves lead to excellent piezoresistive properties of composite.

Alkyl-functionalized graphite oxide nanosheet polydimethylsilicone composites with low percolation threshold (0.63 vol%) have been prepared by Hou et al. [38] through wet mixing method. Low percolation threshold is attributed to high aspect ratio and homogeneous nanosheet dispersion in the polydimethylsilicone. The thickness of functionalized graphene oxide nanosheets was 2.7 nm.

Composites containing 1.19 vol% conductive filler showed the highest piezoresistive sensitivity ($R/R_0 > 400$).

Pressure-sensitive nanocomposites have been made by Soltani et al. [39] from room temperature vulcanizing silicone rubber, graphite nanosheets, and interfacial compatibilizer alkyl ammonium salt. Use of compatibilizer decreased the percolation threshold from 3 to 1 wt% as well as piezoresistive sensitivity from more than 100,000 to around 100 R/R_0 . The decrease of piezoresistive sensitivity is attributed to the high dispersion state of filler throughout the composite leading to insufficient distance between particles to make conductive paths under external pressure.

Sampo Tuukkanen et al. [40] report about the fabrication and characterization stretchable CNT and graphene nanocomposite electrodes on different rubber substrates. Authors used commercially available graphene ink (P3014 Graphene Screen Printing Ink from Innophene Co., Thailand) as well as custom-made CNT ink wich was prepared by mixing CNTs and cellulose derivatives with ultrasonication (obtained from Morphona Ltd., Finland). Both inks were deposited as stretchable electrodes using blade-coating method on four different types of rubber substrates: (1) blend of natural rubber (NR) and butadiene rubber (BR)—NR/BR with 15 phr clay, (2) NR/BR with 25 phr carbon black, (3) nitrile-butadiene rubber NBR unfilled, and (4) was chlorosulfonated polyethylene CSM. These substrates were chosen due to their different chemical structure and mechanical properties. Before the electrode deposition, the substrate rubber samples were stretched reversibly up to 20 % elongation to remove tensile stress softening. After deposition, the graphene film-like electrodes were dried for 7 min and the CNT electrodes for 5 min at 403 K. To obtain the sheet resistances approximately the same for both materials and in such way to make the analysis of the results more consistent, the final thicknesses of the graphene films were approximately 3–5 μm and 1 μm of the CNT films. The electrical resistance of the fabricated sheet electrodes was measured using four-point probe method. Accordingly to classification given in Sect. 2.1., the PTR effect has been found for both types of sheet electrodes. The CNT ink sheets showed good properties for all four rubber substrates. Their electrical resistance before and after the stretching was not changed. In contrary, the graphene ink was highly dependent on the substrate material. High-quality electrodes with low resistances were obtained in the cases of high surface energy rubbers 3 and 4. The graphene ink samples on substrates 1 have some cracks already before stretching but in case of substrate 2, the graphene electrodes contained some bubbles. Authors [40] believe that these faults caused higher resistances both before and after stretching. Authors also conclude that the relative resistance change during the stretching is larger and rubber relaxation after the stretching affects less to the electrical resistance in the case of CNT electrodes. This makes the CNT films more suitable for sensor applications where varying stress is applied to the element. On the other hand, the smaller relative resistance change during the stretching of the graphene electrodes would make them applicable to be used as stretchable electrodes.

Kumar et al. [41] have stated NPR effect for poly(isobutylene-co-isoprene) (IIR)/reduced graphene oxide (RGO) composites with 5 wt% RGO. The RGO was

synthesized from graphite flakes using Improved Graphene Synthesis [42] with subsequent thermal reducing at 473 K temperature for 30 min. (IIR/RGO) composite samples with 5 wt% RGO were prepared by the solution mixing process in tetrahydrofuran (THF) using subsequent ultrasonic treatment for RGO suspension and mechanical mixing of RGO suspension with IIR in THF for 3 h. Thereafter, the mixture was dried at 333 K in vacuum oven until it achieves a constant weight and samples were molded at 433 K for optimum curing time determined by rheometer. SEM, AFM, and XRD investigations showed homogeneous dispersion of RGO in IIR whereas IIR/expanded graphite (EG) composites tested for comparison indicated poor dispersion of EG. The thickness of the sensor sample was 0.1 mm and relative resistance change of the sensor was measured while applying force in the range of 0.05–0.1 kN. Unfortunately, the comprehensive theoretical explanation of the piezoresistivity effect in this material is not given. Authors [41] mentioned only that the resistivity of the composite can change with external pressure due to the construction and destruction of conductive networks as explained in [39].

Very promising results for future development of highly sensitive tactile sensors have got Hodlur and Rabinal [43] by preparing polyurethane foam (PM) with self-assembled graphene layers inside of pores on the surface of polymer. They used the simple method as follows: First, the flexible PF was impregnated with hydrazine hydrate for a minute and washed with distilled water. Home-synthesized graphite oxide (GO) sample was dispersed in distilled water (0.5 mg in 1 ml water) to get GO colloidal solution. Second, the PF was soaked in GO colloidal solution and left to dry for an hour. Third, the PF was saturated with hydrazine hydrate to reduce GO to graphene. At the end it was washed as well as sonicated for few times in distilled and dried in room conditions. Authors [43] chosen for testing PF with approximately 3 wt% graphene. The conductivity of this sample changes by more than 5 orders of magnitude at applied voltage of 1 V if pressure rises from 1.01 to 1.52 atmospheres. So the negative pressure coefficient was stated for this material. Authors believe that such high value of pressure sensitivity can be explained by vertically oriented stacked graphene layers on polyurethane pores inside surface. FTIR analysis and SEM measurements indicates strong chemical bonding between PF surface and graphene flakes in vertically tilt configuration. In our opinion, the evidence for this are a little bit sophisticated because the high-resolution SEM recordings should be limited by the fact that high-energy electron beam is going to burn the PF. In our opinion, more convincing evidences for existence of vertically oriented stacked graphene layers on the inside surface of polyurethane pores should be found in future. We also hope that authors [43] will elaborate more comprehensive numerical model for mechanism of pressure sensing for this very promising material.

Vera Goncalves et al. [44] studied piezoresistive properties of electrically conductive polymer composites made from porous polyether block amide (PEBA 4,033 from “Atofina Chemicals”) and various grades of graphene platelets obtained from “XG Sciences.” Altogether five graphene platelet grades where used: C-750 (length 1–2 μm; thickness 2 nm; surface area 750 m^2/g), M5 (length

5 μm; thickness 6–8 nm; surface area 120–150 m^2/g), M15 (length 15 μm; thickness 6–8 nm; surface area 120–150 m^2/g), M25 (length 25 μm; thickness 6–8 nm; surface area 120–150 m^2/g), and H5 (length 5 μm; thickness 15 nm; surface area 50 m^2/g). The composites were prepared similarly to polymer dissolution method as described previously in Sect. 3. Porous morphology of electrically conductive polymer composite structures was achieved using all graphene platelets except C-750. The reason for this result is not explained in the following paper as well as the authors studied the influence of the remaining various graphene platelet grades on the piezoresisitive properties of their produced porous composites only at one specific concentration of conductive fillers—15 vol%. Therefore it is our responsibility to notify that the further discussed results might be inaccurate for determination of the most suitable graphene platelet grade for production of piezoresistive polymer/nanographite composites since piezoresistivity and conductivity highly depends on the conductive filler geometry and concentration. Composites containing H5 grade graphene exhibited the lowest electrical resistivity; however it did not exhibit any pressure sensitivity. The most promising piezoresistive response was achieved from composites containing M5 grade filler, which as authors highlight exhibited almost linear negative piezoresistive response to pressure up to 0.254 MPa on a log(R)–log(P) plot, but in cyclic loading/unloading conditions sensor exhibited significant hysteresis and resistivity drift due to poor mechanical properties of porous morphology. In Table 1, piezoresistive behavior and sensitivity of the previously mentioned polymer/graphite nanosheet composites are compared.

4.3 Hybrid Polymer/Nanographite Composites

Kim et al. [45] report about the preparation and investigation of nano smart hybrid material based on graphene. However, there is not explanation given why authors named the epoxide/graphene composite (EGC) a hybrid material. The appropriate amounts of graphene (KITECH) were incorporated into the epoxy (KUKDO CHEMICAL Co., YD-128) by direct dispersion into aqueous epoxy using ultrasonic homogenizer. A curing agent, Jeffamine (KUKDO CHEMICAL Co., A-230) was added to the dispersed graphene/epoxy suspension which was then located in a vacuum oven to remove the air. Afterwards the mixed suspension was poured into a silicon mold and cured at room temperature for 24 h and at 80 °C and 120 °C for 2 and 3 h respectively. The sensing element electrodes were made from conductive silver epoxy. The prepared sensor was tightly bonded on a steel beam with superglue to transfer the tensile strain from steel beam to a prepared epoxy/graphene sensor element [45]. Percolation threshold was found to be 3 wt% graphene. It is not shown by authors how percolation threshold was determined and the investigated piezoresistive sample also contains 3 wt% graphene. It is odd since, according to the definition, at percolation thresholds the composite merely starts to become conductive and its resistivity is too large for real piezoresistivity sensor application. The electrical resistance of EGC layer has been measured

Table 1 Comparison of piezoresistive sensitivity of polymer composites based on the graphite nanosheets

Filler	Matrix	Percolation threshold	Piezoresistive behavior	Piezoresistive sensitivity
Alkyl-functionalized graphite oxide (thickness 2.7 nm)	Silicone rubber	0.63 vol%	Positive	$R/R_0 > 400$ under 1.2 MPa [38]
Graphite nanosheets (5–20 μm; 30–80 nm)	Silicone rubber	0.9 vol%	Positive	$R/R_0 = 800{,}000$under 0.7 MPa [15]
Graphite nanoplatelets (thickness 10 nm)	Acrylnitrile butadiene rubber	0.5 phr	Positive	$R/R_0 > 100$ under 6 MPa [20]
Graphite nanosheets (thickness 30–80 nm)	Silicone rubber	3 wt%	Negative	$R/R_0 = 0.00001$ under 1 MPa [39]
Graphite nanosheets (5–20 μm; 30–80 nm)	High-density polyethylene		Negative till 12 MPa	$R/R_0 = 0.15$ under 12 MPa;
			Positive after 12 MPa	$R/R_0 = 800$ under 40 Mpa [37]
Reduced graphite oxide (nanoscale)	poly(isobutylene-co-isoprene)		Negative	$\Delta R/R_0 = 0.5$ under 0.05 kN [41]
Graphite oxide	Polyurethane foam		Negative	R/R_0 ~0.000001 under 52.7 kPa [43]
Graphene platelets (5 μm; 6–8 nm)	Porous polyether block amide		Negative	$R/R_0 = 0.42$ under 245 kPa [44]

versus steel beam deflection. The beam deflection was converted to strain by means of beam theory. In our classification the PTR effect was investigated. Except for some inaccuracies, authors [45] obtained promising results—exactly linear piezoresistivity in the range of 1,000 micro-strain as well as comparatively large gauge factor of 11.4 in comparison with epoxy/MWCNT composite—2.9. Authors also presented interesting explanation of such large gauge factor. If the strain sensor is subjected to tension, the contact resistance between adjacent graphene in conductive channel is increased mainly due to the reduction of the contact area of these overlapping adjacent graphene nanosheets. Based on this hypothesis, authors supposed that higher strain sensitivity of graphene composites can be explained as follows. The larger intercontact area among the graphene nanofillers due to their 2D structure may induce larger contact resistance change than other 1D structure carbon nanotubes. Charge tunneling between adjacent conductive nanoparticles was not discussed in this case.

Very interesting graphene-functionalized carbon nanotube and PVDF matrix composite strain-sensing materials were developed by Varrla Eswaraiah et al. [46]. These materials can be related to the class of hybrid composites. Authors prepared graphene-wrapped CNTs (GWCNTs) from fine ground powders of graphene oxide and alloy hydride (MmNi3) in a quartz tube in a furnace in subsequent argon, hydrogen, argon, acetylene, and argon atmospheres. The prepared graphene-wrapped CNTs were purified by refluxing in concentrated HNO3. Using the ultrasonic-assisted solvent casting method, GWCNTs were dispersed in PVDF matrix as follows: Definite quantity of GWCNTs as well as the corresponding amount of PVDF was dispersed separately in DMF with the help of ultrasonicator for 1 h at room temperature. These two solutions were mixed together by ultrasonicating for 1 h and the mixed solution was transferred into shear mixer and stirred at room temperature at 4,000 rpm for 2 h and at 80 °C for 30 min. The composite solution was taken out from the mixer and transferred into a Petri dish and kept in an oven at 80 °C in vacuum for 6 h to remove the solvent. Automatically peeled off polymer composite films were collected and cut into the required dimensions for further measurements. GWCNTs-based PVDF composite film was attached to one side of the aluminum (Al) specimen using high-strength epoxy to make a perfect bonding between the Al and the nanocomposite film; on the other side, a conventional metallic strain gauge was attached using glue. The specimens were investigated under tensile strain and the PTR linear effect was experimentally determined. Authors [46] compared results with insulating hydroxyl-group-functionalized CNT-based PVDF nanocomposites to show the superior performance of the graphene wrapped over CNT-based PVDF composites. A strain gauge factor of ≈20 has been obtained with 3 wt% conducting graphene wrapped over CNT-based PVDF composites whereas the gauge factor is ≈2 with insulating-molecule-functionalized CNT-based PVDF composites. Authors mentioned three main possible reasons for the piezoresistivity effect: (1) loss of conductive interconnections; (2) a tunneling effect between neighboring fillers, and (3) conductivity change from the deformed graphene-wrapped CNT hybrid. Authors concluded that since the conductance of the composite mainly comes from the nanofiller used and its distribution in the polymer matrix, a change in the number of conductive nanofillers or the loss of contacts in the polymer matrix is responsible in large for the change in resistance of the composite.

5 Development of Polymer/Nanographite Composite Sensor Element Systems for Mechanical Impact Sensing

Most of the pressure sensing systems are created as stiff structures made from brittle materials and therefore their usage is usually limited by ability to endure impact, vibrations, or large deformations. On the other hand, industries like civil and medical engineering, automotive as well as robotics are interested in cheap, reliable sensors without these limitations. In the above-described research, PNGC

was proposed as a potential material for pressure and strain sensor elaboration. In this section, the influence of various nanographite fillers on the piezoresistive properties of PNGC is investigated and based on these results we chose the most suitable compositions for the development of relatively large-scale hyperelastic pressure sensor system (HPSS). Afterward the piezoresistive response of the developed HPSS was measured under external 0.1 and 1 MPa pressure in cyclic loading-unloading conditions; in addition, we determined the processing pressure influence on the piezoresistive sensitivity and behavior of HPSS under 0.1 MPa of pressure.

Two different types of nanographite fillers have been used:

1. 0-dimensional nanostructures—highly structured carbon black Printex XE2 obtained from Degussa®—specific surface area 950 m^2/g, average primary particle diameter 30 nm, DBP absorption 380 ml/100 g;
2. 2-dimensional nanostructures—thermally exfoliated graphite obtained from Kyiv National Taras Shevchenko University. Authors from this university showed that plastic deformation of graphite-epoxy/TEG composites under mechanical loading leads to irreversible changes in the value of normalized resistance R/R_0. The rate of these changes is determined by graphite filler content in epoxy matrix, method of preparation, and composite matrix porosity [47].

Depending on the filler type, two different raw PNGC production methods were used. In the case of HSCB filler, the polyisoprene (PI) and the necessary vulcanization ingredients (sulfur, stearic acid, zinc oxide, and N-Cyclohexyl-2-BenzothiazoleSulfenamide) were mixed with various high-structure carbon black concentrations using roll mixing. The obtained composition further in text is refered to as PICB. In contrast, for TEG filler, a multistep solution mixing method was used:

1. PI with curing ingredients was stirred and dissolved at room temperature for 24 h;
2. dispersion of TEG filler in chloroform (dispersed using ultrasonication with specific power 1 W × 5 min/1 ml to reduce the particle size Fig. 10) was added to the PI solution and stirred for 24 h;
3. obtained mixture was poured into Petri dishes and left for 24 h in drying chamber for chloroform to evaporate;
4. films were homogenized using cold rolling. Obtained compositions are abbreviated as PITEG.

To determine electrical as well as piezoresistive properties for each PNGC composition flat, round-shaped samples (diameter of 18 mm and average thickness of 1 mm) with brass foil electrodes were made by vulcanizing the raw rubber composites in hot stainless steel mold using Rondol thermostated press for 15 min under 3 MPa of pressure at 150 °C. The optimal curing conditions were determined using Monsanto 100 dynamic rheometer. After curing, the samples were shelf aged at room temperature for at least 24 h before any measurements were made.

The electrical conductivity of each PNGC sample was measured using Keithley 6,487 Picoammeter/Voltage source. The piezoresistive effect was determined

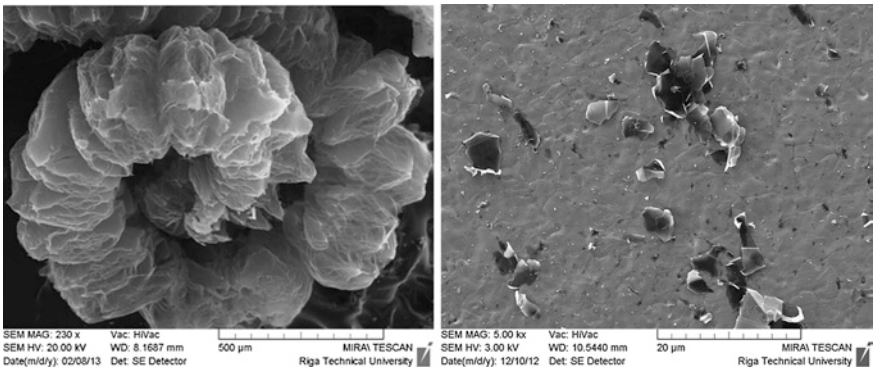

Fig. 10 Scanning electron images of TEG (*left*) and TEG after ultrasound treatment (*right*) particles

using Zwick/Roell Z2.5 universal material-testing machine coupled with Agilent 34970A data acquisition/switch unit. Due to the technical limitations of this measuring equipment, PNGC samples with conductivity lower than 10–8 S/m were not tested for piezoresistivity.

First the electrical conductivity of PNGC samples was determined. Figure 11 shows nanographite filler influence on the percolation transitions of PNGC compositions. The concentration of the conductive fillers is expressed in parts per hundred rubber (phr). PICB composition shows the steepest percolation curve; therefore, theoretically it could be expected for this composition to have the best piezoresistive behavior. Also it should be kept in mind that PICB composites were prepared with a different production method. TEG, on the other hand, is more or less a 2D nanostructure therefore the highest percolation transition in this case could be explained with difficulty to form a continuous conductive network of TEG particles throughout the matrix.

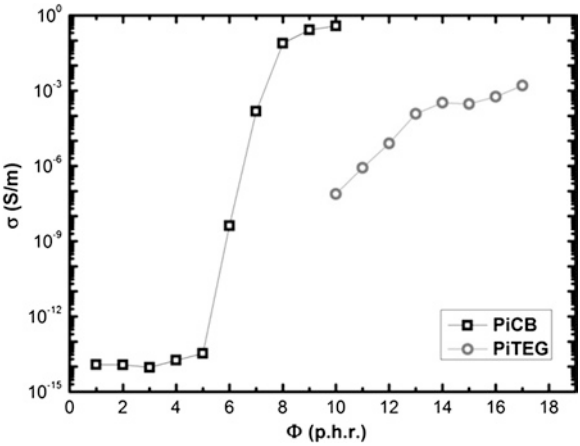

Fig. 11 The electrical percolation transition of PNCC

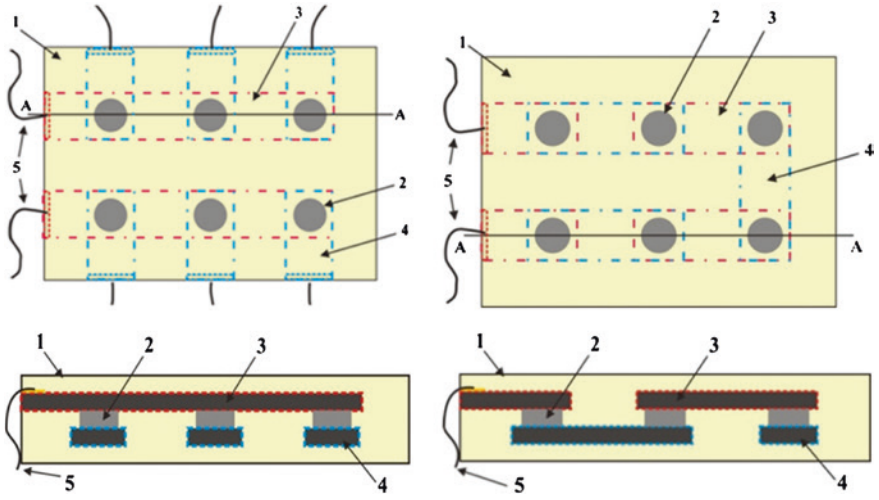

Fig. 12 **a** (left) schematic view of AHPS and schematic AA cross section of AHPS; **b** (right) schematic view of EHPS and schematic AA cross section of EHPS; consisting of : *1* non-conductive outer shell, *2* piezoresistivePiCB, *3* upper layer of conductive PICB, *4* lower layer of conductive PICB, *5* wires with soldered small brass foil plates. The geometrical dimensions of both designed systems were 100 × 70 × 5 mm

The hyperelastic pressure sensor system was made using layered composite design where pressure-sensitive elements were jointed with electrode elements and incorporated into protective nonconductive natural rubber shell (Fig. 12). As the pressure-sensitive elements, PICB with 8 phr CB was used since the piezoresistive sensitivity of this composition under 0.1 MPa was found to be the highest. Since the specific electrical conductivity for the composition PICB with 10 phr CB was high enough, it was used as hyperelastic electrode elements on both sides of sensitive elements. The placement of electrode layers in HPSS was designed to insure that:

1. each of the sensitive elements could be monitored separately (AHPS—addressed hyperelastic pressure sensor system);
2. the sensitive elements were connected in series to provide better piezoresistive sensitivity under external pressure (EHPS—enhanced hyperelastic pressure sensor system);

All HPSS elements were first separately partially vulcanized for 11 min under 3 MPa of pressure at 140 °C to ensure that they could maintain their shape during the final vulcanization when all elements where assembled in designated positions and cured together under 3 MPa of pressure at 150 °C for 20 min. To determine the influence of the vulcanization pressure on the piezoresistive behavior of the sensor, the EHPS elements were semi-vulcanized and the final product was vulcanized into one solid block under 0.5, 1, and 2 MPa of pressure (EHPS 0.5, EHPS 1, and EHPS 2). To connect HPSS to measuring equipment, small wires

with soldered brass foil extensions were added to the side electrode layers. Cross-section of the EHPS system is shown in Fig. 13.

The piezoresistive behavior of EHPS under 0.1 MPa and 1 MPa operational pressures was determined (Fig. 14). As can be seen in Fig. 14, the piezoresistive behavior is very similar under 0.1 and 1 MPa of cyclic operational pressure; however, the piezoresistive sensitivity under 0.1 MPa of pressure is comparatively low (less than 2 %) as well as the piezoresistive behavior under repeated cyclic loading tends to decrease gradually. This can be explained with different speed of electrical relaxation for separate structural PICB elements of EHPS and therefore leads to the decrease of total piezoresistive effect in both ranges of operational pressure.

Figure 15 shows the piezoresistive behavior of EHPS made using different processing pressures under operational 0.1 MPa pressure. One can see that EHPS, which was made using highest processing pressure—3 MPa, appears to be the most piezosensitive. As one can see for small operational pressures (0.1 MPa), the sensitivity of EHPS drops considerably when processing pressure is reduced—this can be explained with improved mobility of electrically conductive particles in vulcanization process, leading to more electrically conductive channels in the composite structure.

Likewise, the piezoresistivity was determined for each AHPS each sensitive element up to 0.1 MPa pressure (Fig. 16). Variance of each element sensitivity at 0.1 MPa pressure is observable.

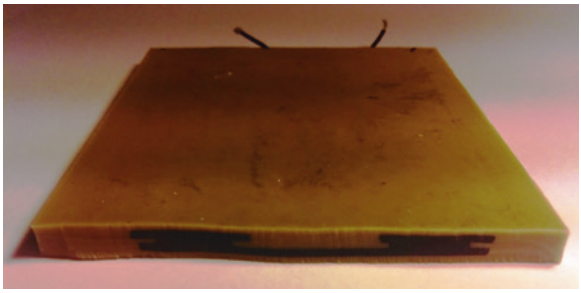

Fig. 13 Cross-section image of EHPS

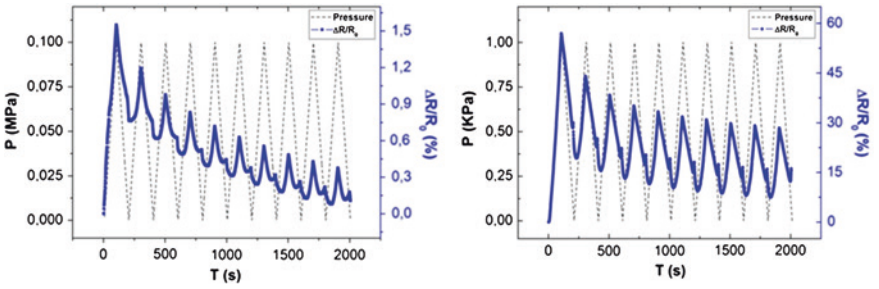

Fig. 14 Piezoresistive behavior of EHPS under cyclic operational pressure up to 0.1 MPa (*left*) and 1 MPa (*right*)

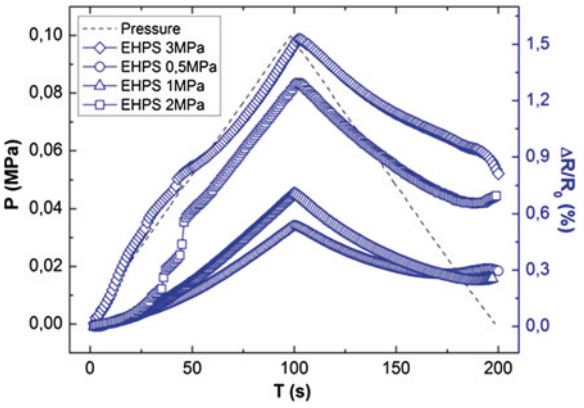

Fig. 15 Piezoresistive behavior of EHPS with different processing pressures under operational pressure of up to 0.1 MPa

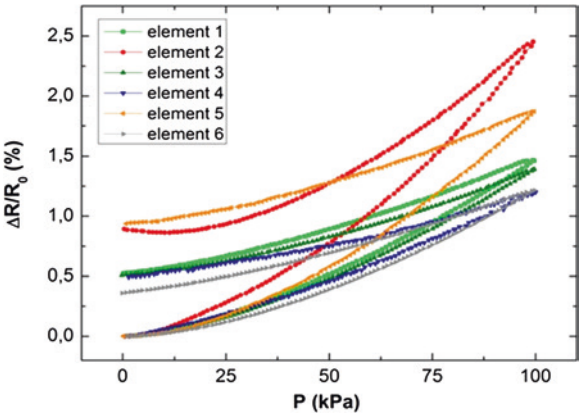

Fig. 16 Piezoresistive behavior of AHPS each sensitive element under operational pressure of up to 0.1 MPa

Similarly to HPSS manufacture, hyperelastic pressure sensor (HPS) with only one sensitive element (HPS) was developed. In Fig. 17 one can see a schematic image of HPS structure. As the pressure-sensitive elements in HPS, the PICB with 8 phr CB or the PITEG with 15 phr TEG were used since the piezoresistive sensitivities of these compositions were found to be the highest. As hyperelastic electrode elements on both sides of sensitive elements PICB with 10 phr filler was used. Small wires with soldered brass foil were added to the hyperelastic electrodes for resistivity monitoring. Finally, all of this was incorporated into protective nonconductive natural rubber shell.

The piezoresistive behavior of HPS with both sensitive elements was determined up to 0.1 MPa pressure (Fig. 18). As seen from Fig. 18, hyperelastic pressure sensor with PITEG sensitive layer shows noticeably higher pressure sensitivity. HPS with PICB-sensitive layer exhibits better effect reversibility. This could be explained as follows—in PITEG and PICB composites conductivity is possible due to tunneling currents between nanographite particles. Since intensity of tunneling currents is highly dependent on the average distance between conductive particles, piezoresistive behavior can be observed under external influences

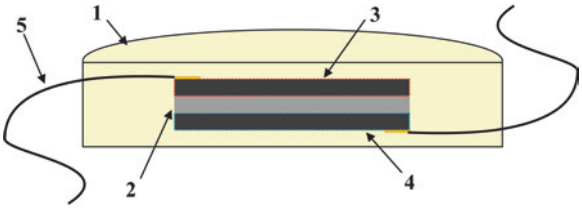

Fig. 17 Schematic view of HPS consisting of: *1* nonconductive outer shell, *2* piezoresistive PiCB or PITEG, *3* upper layer of conductive PICB, *4* lower layer of conductive PICB, *5* wires with soldered small brass foil plates. The geometrical dimensions of designed system was 18 mm in diameter and 5 mm thickness

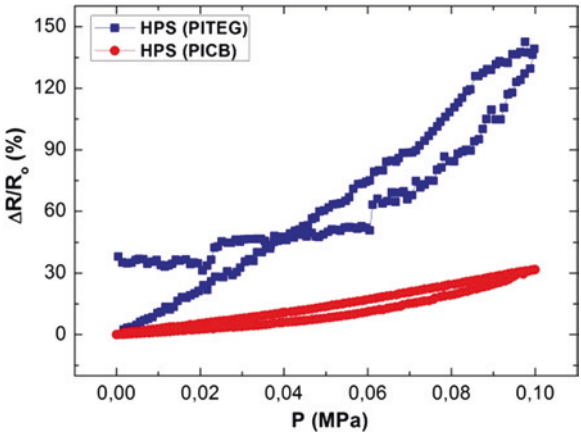

Fig. 18 Piezoresistive behavior of HPS with PITEG- and PICB-sensitive elements under operational pressure of up to 0.1 MPa

(pressure, strain) of PNGC. HSCB particles are believed to have a very complex surface characteristics possibly leading to more than one electrical contact point between two particles when forming conductive channels in PICB composites; therefore, electrical percolation is observed at lower filler concentrations compared to PITEG composites (Fig. 11). However, PITEG composites exhibits higher piezoresistive sensitivity since two TEG particles can form only one electrical contact point between them (due to geometrical nature of two planes) in PITEG-conductive channels leading to reduced electrical shunting of conductive channels when the whole structure is deformed.

6 Summary and Conclusions

Comparatively with other nanographite fillers, both graphene and graphene platelets are rather little used as fillers to elaborate the nanocomposite for mechanical impact sensing; however, in the last 2 years, the number of original papers in this field is rising very sharply [34–36, 40, 41, 43, 44]. One can see from the literature analysis that elastomers are mostly used as matrix material in such kind of

sensitive nanocomposites, because of better sensitivity and comparatively faster recovery of electrical resistivity after reduction of mechanical loading.

At the end of this chapter, we are going to discuss the main strengths and weaknesses of mechanical impact sensing systems made on the basis of polymer/nanographite composites.

As main strengths of rubber-like sensors, we consider:

1. the durability against direct and strong mechanical impact in comparison with brittle piezoceramics or plastic metallic materials;
2. the durability against influence of definite environment factors like humidity, oxidation, etc.;
3. the possibility to adjust the chemical composition of composite material to cover broad dynamical diapason of mechanical stress sensing from few Pa to hundreds of MPa;
4. the cost of materials, relatively simple preparation of sensor material as well as detection of sensors output
5. the possibility to fabricate large and continuous sensing elements integrated in different provable systems.

As significant weaknesses one should mention:

1. the long-drawn recovery processes of small reorientations of polymer chains after mechanical impact that seriously limits the use of such materials for very accurate mechanical strain or stress measurement;
2. as follows from the previous, polymer nanographite composites at the state of the art can be used only for registration or counting of mechanical impacts on sensing element.

The future perspective as well as the challenges in this field we see as follows:

1. development of polymer nanographite composites with permanently aligned graphene 2D particles to improve the sensitivity;
2. elaboration of porous elastomer nanographite composites to improve the sensitivity; and
3. creation of hybrid polymer composites with mixed different allotropes of nanographite, where the sensor material properties will be improved due to the synergy between these fillers.

Acknowledgments This work was partly supported by ESF Grants Nr. 1DP/1.1.1.2.0/13/APIA /VIAA/030 and Nr. 1DP/1.1.1.2.0/13/APIA/VIAA/021

References

1. Hoffman W, Gupta H (2001) Kautchuk und Gummi Kunststoff. Doktor Gupta Verlag, Ratingen.
2. Donnet JB (2003) Nano and microcomposites of polymers elastomers and their reinforcement. Compos Sci Technol; 63:1085-1088.

3. Heo JS, Chung JH, Lee JJ (2006) Tactile sensor arrays using fiber Bragg grating sensors. Sensor Actuat A-Phys 126:312–327.
4. Fortes LM, Gonçalves MC, Almeida RM (2011) Flexible photonic crystals for strain sensing. Opt Mater 33:408-412.
5. Yan C, Ferraris E, Geernaert T, Berghmans F, Reynaerts D (2012) Characterisation of tactile sensors based on fibre Bragg gratings towards temperature independent pressure sensing. Procedia Engineering 47:1402-1405.
6. Lee B, Roh S, Park J (2009) Current status of micro- and nanostructured fiber sensors. Opt Fiber Technol 15:209-221.
7. Staufer D, Aharony A (1992) Introduction into percolation theory. Taylor & Francis, Washington.
8. Roldughin VI, Vysotskii VV (2000) Percolation properties of metal-filled polymer films, structure and mechanisms of conductivity. Prog Org Coat 39:81-100.
9. Balberg I, Azulay D, Toker D, Millo O (2004) Percolation and tunneling in composite materials. Int J Mod Phys B 18(15):2091-2121.
10. Knite M, Teteris V, Kiploka A, Kaupuzs J (2004) Polyisoprenecarbon black nanocomposites as strain and pressure sensor materials. Sensor Actuat A-Phys 110:142–149.
11. Rocha JG, Paleo AJ, Ferrie WJ, van Hattum WJ, Lanceros-Mendez S (2013) Polypropylene-carbon nanofiber composites as strain-gauge sensor. IEEE Sens J 13(7):2603-2609.
12. Laukhin V, Laukhina E, Lebedev V, Pfattner R, Rovira C, Veciana J (2011) Flexible all-organic highly tenzo-resistive bi layer films as weightless strain and pressure sensors for medical devices. In: Proceedings of the Second International Conference on Sensor device Technologies and Applications, SENSORDEVICES 2011, p 151.
13. Zhang XW, Pan Y, Zheng Q, Yi XS (2000) Time dependence of piezoresistance for the conductor filled polymer composites. J Polym Sci Pol Phys 38:2739-2749.
14. Stassi S, Cauda V, Canavese G, Pirri CF (2014) Flexible Tactile Sensing Based on Piezoresistive Composites: A Review. Sensors 14:5296-5332.
15. Chen L, Chen G, Lu L (2007) Piezoresistive Behavior Study on Finger Sensing Silicone Rubber/Graphite Nanosheet Nanocomposites. Adv Funct Mater 17:898-904.
16. Flandin L, Hiltner A, Baer E, (2001) Interrelationships between electrical and mechanical properties of a carbon black filled ethylene-octene elastomer. Polymer 42:827-8238.
17. Simmons JG (1963) Electric tunnel effect between dissimilar electrodes separated by thin insulating film. J Appl Phys 34(9):2581-2590.
18. Zavickis J, Knite M, Podins G, Linarts A, Orlovs R (2011) Polyisoprene – nanostructured carbon composite – a soft alternative for pressure sensor application. Sensor Actuat A-Phys 71:38-42.
19. Luheng W, Tianhuai D, Peng W (2009) Influence of carbon black concentration on piezoresistivity for carbon black filled silicone rubber composite. Carbon 47:3151-3157.
20. Al-solamya FR, Al-Ghamdib AA, Mahmoud WE (2012) Piezoresistive behavior of graphite nanoplatelets based rubber nanocomposites. Polym Advan Technol 23:478-482.
21. Zheng S, Deng J, Yang L, Ren D, Huang S, Yang W, Liu Z, Yang M (2014) Investigation on the piezoresistive behavior of high density polyethylene/carbon black films in the elastic and plastic regimes. Compos Sci Technol 97:34-40.
22. Knite M, Klemenok I, Shakale G, Teteris V, Zicans J (2007) Polyisoprene-carbon nano-composites for application in multifunctional sensors. J Alloy Compd 434–435:850-853.
23. Kanoun O, Müller C, Benchirouf A, Sanli A, Dinh TN, Al-Hamry A, Bu L, Gerlach C, Bouhamed A (2014) Flexible Carbon Nanotube Films for High Performance Strain Sensors. Sensors 14:10042-10071.
24. Bauhofer W, Kovacs JZ (2009) A review and analysis of electrical percolation in carbon nanotube polymer composites. Compos Sci Technol 69:1486-1498.
25. Zavickis J, Linarts A, Knite M (2011) The downshift of the electrical percolation threshold in polyisoprene nanostructured carbon composites. Energetika 8:44-49.
26. Knite M, Tupureina V, Fuith A, Zavickis J, Teteris V (2007) Polyisoprene – multi-wall carbon nanotube composites for sensing strain. Mat Sci Eng C-Biomim 27:1125-1128.

27. Park S, Ruoff RS (2009) Chemical methods for the production of graphenes. Nat Nano 4(4):217-224.
28. Grehov V, Kalnacs J, Matzui L, Knite M, Murashov A, Vilken A (2013) Nitrogen Ad-sorption by Thermoexfoliated Graphite. Latvian Journal of Physics and Technical Sciences 1:58-65.
29. Chiacchiarelli LM, Rallini M, Monti M, Puglia D, Kenny JM, Torre L (2013) The role of irreversible and reversible phenomena in the piezore-sistive behavior of graphene epoxy nanocomposites applied to structural health monitoring. Compos Sci Technol 80:73-79.
30. Knite M, Zavickis J, Sakale G, Ozols K, Linarts A (2013) Advanced smart polymer/nanographite composites for environmental pollution control. Green Design, Materials and Manufacturing Processes - Proceedings of the 2nd International Conference on Sustainable Intelligent Manufacturing, SIM 2013 p 587-592.
31. Knite M, Teteris V, Kiploka A (2003) The effect of plasticizing agent on strain induced change of electric resistivity of carbon polyisoprene nanocomposites. Mater Sci Eng C 23(6–8):787-790.
32. Knite M, Hill AJ, Pas SJ, Teteris V, Zavickis J (2006) Effects of plasticizer and strain on the percolation threshold in polyisoprene carbon nanocomposites: positron an-nihilation lifetime spectroscopy and electric resistance measurements. Mater Sci Eng C 26:771-775.
33. Knite M, Zavickis J (2009) Prospective polymer composite materials for applications in flexible tactile sensors. In: Rodic AD (ed) Contemporary robotics – challenges and solutions, In-The, India, p 99-128.
34. Kumar SK, Ponnamma D, Thomas S, Grohens Y (2014) Evolution from graphite to graphene elastomer composites. Prog Polym Sci 39:749-780.
35. Garima M, Vivek D, Kyong YR, Soo-Jin P, Wi RL (2014) A review on carbon nanotubes and graphene as fillers in reinforced polymer nanocomposites. J Ind Eng Chem in press: http://dx.doi.org/10.1016/j.jiec.2014.03.022.
36. Das TK, Prusty S (2013) Graphene-based polymer composites and their applications. PolymPlast Technol 52:319-331.
37. Lu J, Chen X, Lu W, Chen G (2006) The piezoresistive behaviors of polyeth-ylene/foliated graphite nanocomposites. Eur Polym J 42:1015-1021.
38. Hou Y, Wang D, Zhang XM, Zhao H, Zha JW, Dang ZM (2013) Positive piezoresistive behavior of electrically conductive alkyl-functionalized graphene/ polydime-thylsiliconenanocomposites. J Mater Chem C 1:515-521.
39. Soltani R, Katbab AA (2010) The role of interfacial compatibilizer in controlling the electrical conductivity and piezoresistive behavior of the nanocomposites based on RTV silicone rubber/graphite nanosheets. Sensor Actuat A-Phys 163:213-219.
40. Tuukkanen S, Hoikkanen M, Poikelispaa M, Honkanen M, Vuorinen T, Kakkonen M, Vuorinen J, Lopo D (2014) Streching of solution processed carbon nanotube and graphene nanocomposite films on rubber substrates. Synt Met 191:28-35.
41. Kumar SK, Castro M, Saiter A, Delbreilh L, Feller JF, Thomas S, Grohens Y (2013) Development of poly(isobutylene-co-isoprene)/reduced graphene oxide nanocomposites for barrier, dielectric and sensing applications. Mater lett 96:109-112.
42. Marcano DC, Kosynkin DV, Berlin JM, Sinitskii A, Sun Z, Slesarev A, Alemany LB, Lu W, Tour JM (2010) Improved Synthesis of Graphene Oxide. ACS Nano 4(8):4806-4814.
43. Hodlur RM, Rabinal MK (2014) Self assembled graphene layers on polyurethane foam as a highly pressure sensitive conducting composite. Compos Sci Technol 90:160-165.
44. Goncalves V, Brandao L, Mendes A (2014) Development of porous polymer pressure sensors incorporating graphene platelets. Polym Test 37:129-137.
45. Kim YJ, Cha JY, Ham H, Huh H, So DS, Kang I (2011) Prepartion of piezoresistive nano smart hybrid material based on graphene. Curr Appl Phys 11:350-352.
46. Eswaraiah V, Aravind SSJ, Balasubramaniam K, Ramaprabhu S (2013) Graphene functionalized carbon nanotubes for conducting polymer nanocomposites and their improved strain sensing properties. Macromol Chem Physic 214:2439-2444.
47. Vovchenko L, Lazarenko A, Matzui L, Zhuravkov A (2012) The effect of mechanical stress on electric resistance of nanographite-epoxy composites. Physica E 44:940-943.